




Prediction of Fourier Amplitude Spectrum of Ground Motion in Mexico City from Subduction Thrust Earthquakes

Danny Arroyo^{*1}, Mario Ordaz² and Shri K. Singh³

Abstract

Mexico City, one of the largest cities in the world, experiences frequent, devastating interplate earthquakes that originate on the subduction thrust along the Pacific coast of Mexico more than 250 km away. A notorious example is the 19 September 1985 Michoacán earthquake (M_w 8.0) which killed ~ 10,000 persons and caused wide-spread destruction in the city. The main cause of seismic damage in Mexico City is its subsoil that amplifies the ground motion. In view of the seismic hazard faced by the city, a reliable estimation of ground motion during future earthquakes is of vital importance. We present a new ground motion prediction equation (GMPE) for the Fourier amplitude acceleration spectrum (FAS) from subduction thrust earthquakes along the Pacific coast of Mexico at the reference station, CU, located in the firm zone of Mexico City. The GMPE is derived *via* Bayesian regression analysis and is based on an enlarged set of recordings (1965-2020; 40 earthquakes; $250 \leq R \leq 500$ km; $5 \leq M_w \leq 8.0$). An important feature of the new GMPE is that it includes a term to model different attenuation along different ray paths. The inclusion of this term leads to a reduction in the aleatory variability of the GMPE, particularly at high frequencies. Since spectral amplification of seismic waves with respect to CU is known at many sites in the city, the FAS at these sites can be computed if it is known at CU. The new GMPE has been incorporated in a fully Fourier-based probabilistic seismic hazard analysis of Mexico City.

Key words: GMPE, FAS, subduction earthquakes, Bayesian analysis.

Resumen

La CDMX, una de las ciudades más grandes del mundo, ha sufrido continuamente sismos destructivos que se originan en la interfaz de la zona de subducción en la costa del Pacífico a más de 250 km de distancia. Un ejemplo notable es el gran sismo de Michoacán del 19 de septiembre de 1985 el cual devastó la ciudad y provocó más de 10,000 víctimas. La causa principal de los daños es la gran amplificación del movimiento del suelo que se presenta en la CDMX. En vista del nivel de peligro sísmico a que está expuesta la ciudad es necesario contar con estimaciones precisas del movimiento del suelo durante eventos sísmicos futuros. Se presenta un modelo de atenuación (GMPE) del espectro de amplitudes de Fourier de la aceleración (FAS) del movimiento del suelo, en la estación de Ciudad Universitaria (CU) en la CDMX, durante sismos en la interfaz de subducción a lo largo de la Costa del Pacífico Mexicano con mecanismo de falla inverso. Se consideran registros entre 1965 a 2020 durante 40 sismos con magnitudes entre 5 y 8 a distancias entre 250 km y 500 km, lo cual representa un incremento considerable de registros respecto a los estudios previos. Como método de regresión se utilizó un esquema de regresión Bayesiano. Una característica importante del modelo propuesto es que incluye términos para modelar la atenuación a lo largo de diferentes trayectorias, se observó que la inclusión de estos términos conduce a una reducción en la variabilidad aleatoria del GMPE, particularmente en altas frecuencias. Dado que la amplificación de las ondas sísmicas con respecto a la estación CU se conoce en muchos sitios instrumentados en la CDMX es posible estimar el FAS en estos sitios si se conoce el FAS en la estación CU. El modelo propuesto ha sido incorporado en un análisis de peligro sísmico basado en el uso de FAS y ha dado lugar a los espectros de diseño sísmico de la nueva versión del Reglamento de Construcciones de la CDMX.

Palabras clave: Modelo de atenuación, espectro de amplitud de Fourier, sismos de subducción, análisis de regresión Bayesiano.

Received: June 21, 2023; Accepted: January 20, 2024; Published on-line: April 1, 2024.

Editorial responsibility: Dr. Sreenath Vemula

* Corresponding author: Arroyo, Danny. E-mail: aresda@azc.uam.mx

¹ Departamento de Materiales. Universidad Autónoma Metropolitana.

² Instituto de Ingeniería. Universidad Nacional Autónoma de México.

³ Instituto de Geofísica. Universidad Nacional Autónoma de México.

<https://doi.org/10.22201/igeof.2954436xe.2024.63.2.1717>

1. Introduction

Mexico City and the surrounding metropolitan area, home of nation's 40% population, experiences frequent, devastating interplate earthquakes that originate on the subduction thrust along the Pacific coast of Mexico more than 250 km away. A notorious example is the 19 September 1985 Michoacán earthquake (M_w 8.0) which killed ~ 10,000 persons and caused wide-spread destruction in the city (Anderson *et al.*, 1986). The city is also prey to intraslab, normal-faulting earthquakes in the subducted Cocos plate that may occur at hypocentral distances as close as 120 km. A recent example of this type of event is the 19 September 2017 Puebla-Morelos earthquake (M_w 7.1) which caused severe damage to the city and death of about 220 persons (Singh *et al.*, 2018). Additionally, the city is exposed to seismic hazard from local and regional earthquakes in the Trans-Mexican Volcanic Belt within which Mexico City is situated.

The main cause of damage in Mexico City from interplate and intraslab earthquakes is its subsoil that amplifies the ground motion (Rosenblueth, 1953; Anderson *et al.*, 1986; Celebi *et al.*, 1987; Singh *et al.*, 1988a, 1988b; Ordaz and Singh, 1992). From geotechnical perspective the subsoil is divided in three zones: the lake-bed zone (consisting of 30 to 80 m deposit of highly-compressible, high-water content clay underlain by resistant sands); the hill zone (comprising of a surface layer of lava flows and volcanic tuffs); and the transition zone (composed of alluvial sandy and silty layers with occasional intervals of clay layers). Seismic waves trapped in the soft layers of the transition and lake-bed zones are greatly amplified at frequencies between 0.2 to 1 Hz. The buildings whose natural periods coincide with the dominant period of the subsoil are highly vulnerable to earthquake ground motion.

In view of the seismic hazard faced by the city, a reliable estimation of ground motion during future earthquakes is of vital importance. Following the 1985 Michoacán earthquake, the occurrence of a great earthquake, $M_w \geq 8$, in the Guerrero seismic gap became a major concern of seismologists and earthquake engineers. Ordaz *et al.* (1993) applied a technique of summation of empirical Green's function (EGF) (Joyner and Boore 1986) to estimate ground motions in Mexico City from a postulated M_w 8.2 earthquake in the gap. Later, Ordaz *et al.* (1995) developed an improved scheme of random summation of EGF and re-estimated the ground motions. Kanamori *et al.* (1993) used several recordings as EGFs and, assuming different rupture scenarios and ω^2 -source model, estimated ground motion at a site in Mexico City from an M_w 8.0 earthquake. While the EGF technique is very powerful since it automatically accounts for path and site effects, its application is limited by the availability of adequate EGFs.

An alternative approach that has been pursued is to estimate *FAS* at sites in Mexico City. This is facilitated by the fact that a strong-motion station, CU, located on basalt lava flows at the main campus of National Autonomous University of Mexico (UNAM) in Mexico City, has been in continuous operation since 1964, recording earthquakes during the past 59 years. The extensive recorded dataset has been used to derive ground motion prediction equation (GMPE) for *FAS* at CU (Castro *et al.* 1988, Ordaz *et al.*, 1994). On the other hand, spectral amplifications of ground motion at other sites in the city have been computed with respect to the recordings at CU (Ordaz *et al.*, 1988; Singh *et al.*, 1988b; Reinoso and Ordaz, 1999). To a first order, the spectral amplification at a site in the lake-bed or the transition zone is independent of the magnitude, epicentral distance, depth, and azimuth of the source. Thus, if the *FAS* of the ground motion of an earthquake at CU is known (either from its recording or from the GMPE), then the spectrum can be estimated at all sites in the city whose spectral amplification is known. An application of stochastic theory (Boore, 2003), along with an estimation of the duration of the intense part of the ground motion, then yields the expected ground motion parameters in the city. This empirical approach has been validated for the Valley of Mexico by Ordaz *et al.* (1988) and Reinoso and Ordaz (2001). The approach is very useful in practical applications (Ordaz *et al.*, 2017); it also circumvents the complex wave-propagation phenomenon of seismic waves in a poorly known shallow crustal structure of the valley (Cruz-Atienza *et al.*, 2016).

Since 1994 when the last GMPE for *FAS* at CU was derived, the quality and quantity of useful strong motion (SM) recordings at this station have significantly improved. Because the *FAS* at CU plays such an important role in practical applications, we take advantage of the enlarged dataset to construct a new GMPE. Similar to Ordaz *et al.* (1994) we follow the Bayesian approach in the regression analysis which allows for inclusion of knowledge not directly derived from observed data. Analysis based on the enlarged and improved dataset results in a significant reduction of aleatory variability of the GMPE with respect to the previous GMPE (Ordaz *et al.*, 1994). Guided by the observed residuals, we further modify the model to include the variation of attenuation along different ray paths. We find that this simple modification leads to a reduction in the aleatory variability of the GMPE, especially at frequencies greater than 1 Hz.

2. Data

We searched for SM recordings at CU from shallow-dipping thrust faulting earthquakes on the plate interface. Near-trench earthquakes which are known to be deficient in high-frequency

radiation (Shapiro *et al.*, 1998; Iglesias *et al.*, 2003; Singh *et al.*, 2016), were excluded from the analysis. The remaining dataset comprises of 40 earthquakes recorded between 1965 and 2020. They are listed in Table 1 along with their magnitude (M_w), depth (H) and epicenter. These parameters were taken from published

papers if available; otherwise M_w and H were obtained from the Global CMT catalog (<https://www.globalcmt.org>) and the epicentral location was taken from the catalog of National Seismological Service (SSN; <http://www.ssn.unam.mx/doi/networks/mx/>). Table 1 also lists the closest distance from CU

Table 1. List of earthquakes analyzed in this study. Last 3 earthquakes were not used in the regression analysis

Date	Latitude	Longitude	M_w	Depth, km	R_{rup} , km
23/08/1965	16.28	-96.02	7.45	16	446
03/02/1968	16.67	-99.39	5.9	16	292
02/08/1968	16.25	-98.08	7.2	16	339
01/02/1976	17.15	-100.23	5.6	16	263
07/06/1976	17.45	-101.46	6.4	29	311
07/06/1976	17.036	-99.745	6.6	11	251
29/11/1978	16.00	-96.69	7.6	16.1	419
14/03/1979	17.46	-101.46	7.55	26.7	285
07/06/1982	16.516	-98.339	6.9	18.6	310
07/06/1982	16.424	-98.253	6.9	10.7	322
19/09/1985	18.073	-102.754	8.0	21.3	300
21/09/1985	17.62	-101.82	7.6	20.8	302
30/04/1986	18.361	-103.045	7.0	20.7	403
08/02/1988	17.4	-101.22	5.9	16	299
25/04/1989	16.795	-99.275	6.9	15	266
11/05/1990	17.14	-100.8	5.6	15	294
31/05/1990	17.14	-100.86	5.9	26	297
14/09/1995	16.752	-98.667	7.4	21.8	264
16/12/1997	15.70	-99.04	6.0	16	398
03/02/1998	15.69	-96.37	6.3	24	495
11/07/1998	17.25	-101.54	5.5	24.1	337
12/07/1998	16.83	-100.44	5.5	15	305
22/01/2003	18.60	-104.22	7.5	26	505
01/01/2004	17.30	-101.36	5.7	20.4	319
01/01/2004	17.34	-101.42	6.1	15	318
31/01/2009	17.66	-101.94	5.2	12	343
30/06/2010	16.24	-97.99	6.3	17.8	358
20/03/2012	16.264	-98.457	7.5	15.4	318
11/04/2012	17.9217	-103.068	6.7	20.5	426
21/08/2013	16.7527	-99.5812	6.2	23.3	283
18/04/2014	17.15	-100.845	7.3	18.9	275
08/05/2014	17.163	-100.819	6.5	21.3	287
10/05/2014	17.15	-100.845	6.1	20.7	294
24/05/2014	16.2002	-98.4073	5.7	16.2	354
08/05/2016	16.323	-97.8773	5.9	23.9	357
27/06/2016	16.208	-98.003	5.6	21.3	366
16/02/2018	16.218	-98.0135	7.2	20	345
17/02/2018	15.8438	-97.9887	6.0	16.7	402
19/02/2018	16.2477	-97.775	5.9	23.8	369
23/06/2020	15.8033	-96.1337	7.4	21.5	480
08/09/2021	16.767	-99.951	7.0	15.0	276
19/09/2022	18.220	-103.290	7.6	15.0	453
22/09/2022	18.050	-103.120	6.7	12.0	453

to the rupture area (R_{rup}). M_w of the dataset ranges between 5.0 and 8.0 and R_{rup} between 250 km and 500 km. Figure 1 shows the magnitude-distance plot. The figure identifies events included in the previous study (Ordaz *et al.*, 1994) while Figure 2 shows the corresponding M_w and R_{rup} histograms

The recent Acapulco earthquake of 08/09/2021 (M_w 7.0) and Michoacán - Colima earthquakes of 19/09/2022 (M_w 7.6) and 22/09/2022 (M_w 6.7), which are listed in Table 1, were not included in the regression analysis. They were used to check the validity of the new model. Figure 3 gives a map showing epicenters and magnitudes of all earthquakes, and their ray paths to CU.

SM recordings before 1985 were made by analog accelerographs. The digitized and processed data of these events are available at 50 sps. Beginning 1985 the earthquakes were recorded by digital accelerographs at 100 sps and/or 250 sps. All recordings were baseline corrected and bandpass filtered between 0.1 and 10 Hz. A 5% cosine taper is applied before computing the spectrum which is then smoothed by a 1/6 octave filter. FAS used in the regression is the quadratic mean of the two horizontal components as has been considered in previous GMPE studies in Mexico (Garcia *et al.* 2005, Arroyo *et al.* 2010).

3. The Model

Similar to Ordaz *et al.* (1994), our starting model is based on the solution of a point dislocation in an infinite space. Under far-field approximation and in the presence of anelastic attenuation and site effect, the Fourier acceleration amplitude spectrum, FAS , of the ground motion of an earthquake of seismic moment M_0 (moment magnitude M_w) at distance R_{rup} may be written as:

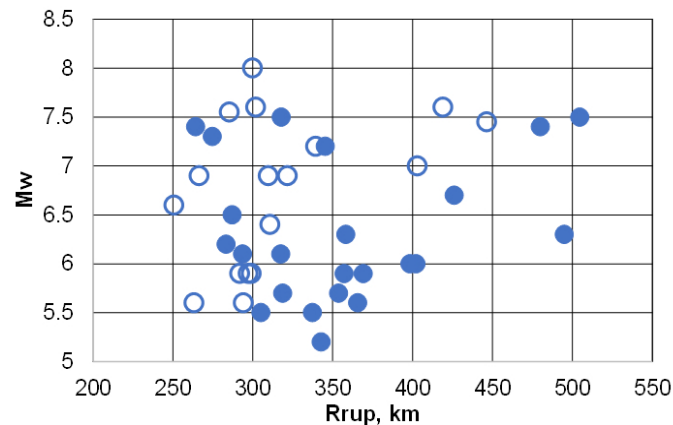


Figure 1. $M_w - R_{rup}$ distribution of the data analyzed in this study. Open circles identify the events considered by Ordaz *et al.* (1994).

$$FAS(M_0, R_{rup}, f) = CG(R_{rup}) \{f^2 M_0(f)\} \left\{ e^{-\frac{\pi f R_{rup}}{\beta Q(f)}} \right\} \quad (1)$$

where C is a constant, $Site(f)$ accounts for the site effect, $Q(f)$ is the quality factor. $G(R_{rup})$ is the geometric spreading function defined by:

$$G(R_{rup}) = \begin{cases} \frac{1}{R_{rup}} & \text{if } R_{rup} \leq R_x \\ \frac{1}{R_x} \left(\frac{R_{rup}}{R_x}\right)^{-0.5} & \text{if } R_{rup} > R_x \end{cases}$$

In common with previous studies in the region, we set $R_x = 100$ km. $\dot{M}_0(f)$ in equation 1 is the moment rate function. For Brune ω^2 -source model (Brune, 1970), $\dot{M}_0(f) = M_0 f_c^2 / (f^2 + f_c^2)$ and $f_c = 4.9 \times 10^6 \beta (\Delta\sigma / M_0)^{1/3}$ where M_0 is in dyne-cm, β is shear-wave velocity at the source in km/sec, and $\Delta\sigma$ is the stress drop in bar. M_w is related to M_0 by $M_w = 2/3 \log M_0 - 10.71$. For regression analysis we recast equation 1 in the following function form:

$$\ln(FAS) = a_1 + a_2 M_w + \ln(G(R_{rup})) + a_3 R_{rup} \quad (2)$$

where a_1 , a_2 and a_3 are coefficients to be determined by regression analysis. The functional form in equation (2) is based on the Brune's point-source model and it lacks terms that account for near source effects. However, given that the earthquakes analyzed herein are always generated at sources located at distances larger than 200 km we found that the functional form in equation (2) leads to reasonable results.

The regression analysis uses the Bayesian technique in which the regression coefficients and standard deviation of the residuals are considered random variables whose prior probability density is known and the prior densities are updated with observations using Bayes' theorem. A detailed discussion of the Bayesian framework can be found elsewhere (e.g., Broemling, 1985; Ordaz *et al.*, 1994). The prior information required by the Bayesian scheme was set as follows. It is assumed that regression coefficients follow a multivariate normal distribution with parameters μ (vector location) and Σ (covariance matrix). In addition, we supposed that the precision of the residuals follows a Gamma distribution with parameters λ (rate) and k (shape).

The elements of the vector location parameter are the prior mean value of the regression coefficients and they were set as follows: for a_1 we set its prior mean value to 1 to set the prior mean value of a_2 we generated a set of synthetic FAS from the Brune source model with $\beta = 3.5$ km/s and $\Delta\sigma = 100$ bar for

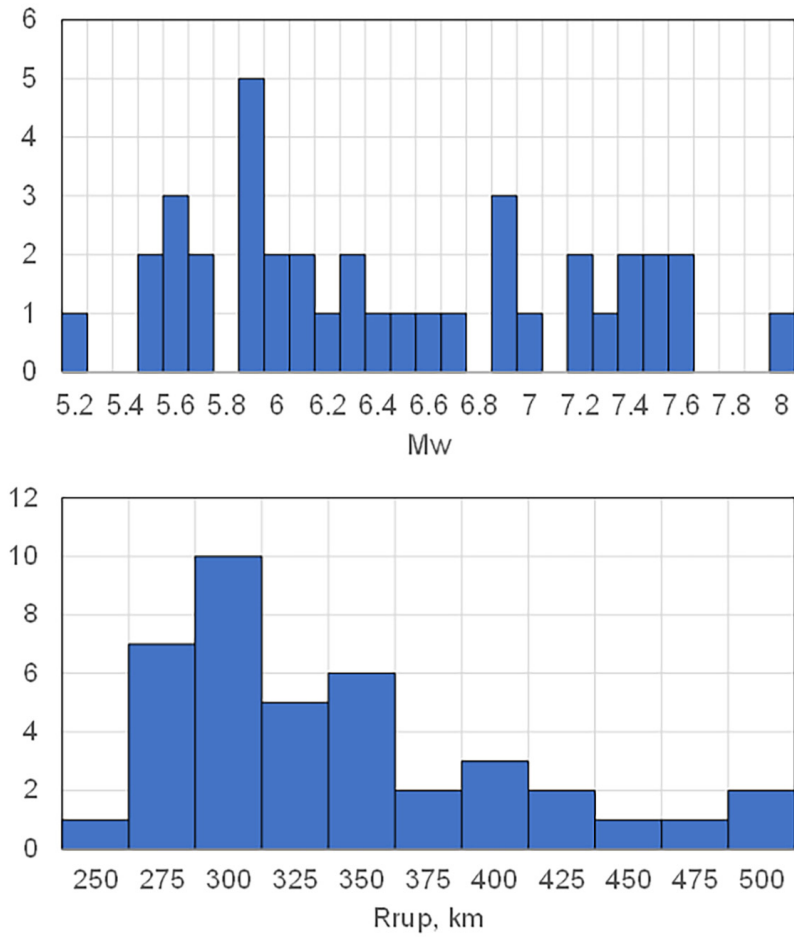


Figure 2. M_w and R histograms for the dataset in Figure 1.

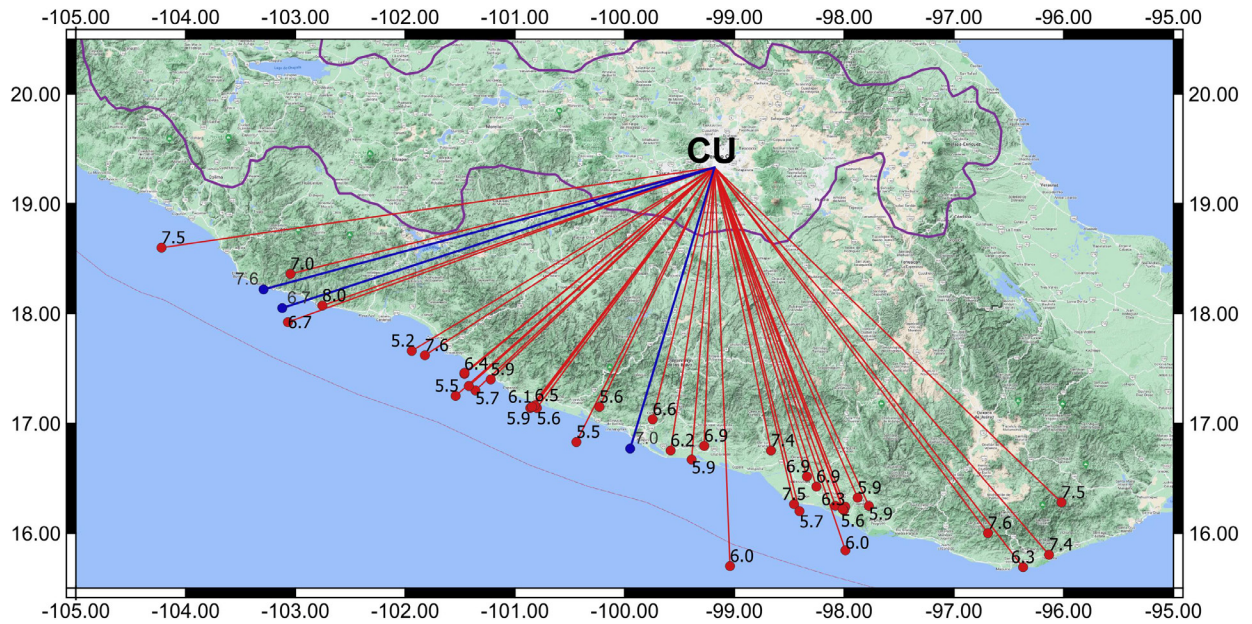


Figure 3. Map showing epicenters and magnitudes of the earthquakes considered in this study. Raypaths to CU are shown in straight lines. Blue dots are 3 recent events which were not included in the regression analysis. Violet contour encloses the Trans Mexican Volcanic Belt.

different M_w and R_{rup} combinations and performed a regression analysis to define the prior mean values a_2 . The prior mean value of the coefficient a_3 was obtained from:

$$a_3' = \frac{-\pi f}{\beta Q(f)} \quad (3)$$

where a_3' is the prior mean value of a_3 . We take $Q(f)=273 f^{0.66}$ reported for the region by Ordaz and Singh (1992).

The elements of the covariance matrix were set as follows: we suppose that, a priori, the regression coefficients are uncorrelated then the covariance matrix was set as a diagonal matrix. The elements in the diagonal of the covariance matrix are the variance of each regression coefficient, we assigned a large variance to a_1 because we decided to let it free during the regression analysis, to define the variance of a_2 we suppose a coefficient of variation equal to 0.3 and to define the variance of a_3 we suppose a coefficient of variation equal to 0.7.

The method also requires the parameters of the prior density of the precision of the residuals ($1/\sigma^2$), we suppose that the prior mean value of σ was equal to 0.7, a value commonly reported in the literature of GMPEs, and we assumed a variance equal to unity, from the properties of the gamma distribution this leads to $\lambda=2.23$ and $k=0.606$.

We emphasize that the prior information for our model comes from a physical model. This is an important characteristic of the model since this assures that in regions of scarce data the predictions will be close to a reasonable physical model.

We performed the regression analysis at 84 frequencies between 0.1 and 10 Hz. We examined the normalized residuals (*i.e.*, the ratio of residuals to their standard deviation) for this model and we noted that the model systematically overestimated or underestimated observations for certain ray paths as shown in Figure 4 (although not shown, similar trends were observed at other frequencies). To study the dependence of the residuals on the ray path, we grouped the events in 5 bins of 300 each. The angles defining the bins are illustrated in Figure 5. The average normalized residual was computed for each bin. The results are summarized in Figure 6 which reveal that for a given frequency the residuals for some paths may be systematically different than residuals for other ray paths. We attribute these trends to the difference in the anelastic attenuation along different ray paths. To account for this variation, we modified the initial functional form in equation 2 to a new one:

$$\ln(FAS) = a_1 + a_2 M_w + \ln(G(R_{rup})) + \sum_{i=1}^5 d_i c_i R_{rup} \quad (4)$$

where a_1 , a_2 , and c_i are now the coefficients to be determined by regression analysis and d_i is a dummy variable which equals 1 if

$0^\circ \leq \theta < 30^\circ$, 0 otherwise, d_2 is a dummy variable which equals 1 if $30^\circ \leq \theta < 60^\circ$, 0 otherwise, and so on. We tried different number of bins in our analysis and noted that as the number of bins increases the σ values decrease but the regression tends to be unstable because overfitting. We decided to set the number of bins to five because we obtain a model that yields realistic predictions, since many bins lead to extreme variation in the predictions that are physically unrealistic.

We set the prior mean value of c_i equal to a_3' (equation 3). For set the covariance matrix we assign a coefficient of variation equal to 0.5 for c_1 and c_3 and a value of 0.8 to the coefficient of variation for c_2 , c_4 and c_5 . We set different prior coefficients of variation to c_i to leave them as free as possible during the regression analysis but avoiding positive values that are physically untenable.

The coefficients of the proposed model and the standard deviation of the residuals in natural logarithmic units (σ) are given in Table 2. In Figures 7, 8 and 9 we compare prior probability density functions and posterior probability density functions for the regression parameters for $f=0.5$, 1 and 5 Hz. The effect of the data on the updating of the prior densities is evident. Figures 10 and 11 show normalized residuals for different frequencies as a function of M_w and R_{rup} . We show a linear trendline for the residuals. As the small values of the slope of the trendline reveal, the residuals tend to be unbiased with respect to M_w and R_{rup} . Figure 12 show similar maps to those in Figure 4 but for the proposed model. In Figure 13 we compare average normalized residuals for different θ bins. As expected, the residuals are nearly independent of θ . For the proposed model the mean residual in the bins is not reduced to zero because, as mentioned earlier, the coefficients c_i are not free during the regression analysis; their values are controlled by the prior mean value in some degree to avoid overfitting. Although some bias persists for some bins at frequencies < 1 Hz, our model yields realistic predictions, because differences in predictions among different bins are physically realistic.

In future, as the number of recordings increases, it would be possible to let the coefficients free during the regression to correct the bias for all bins in the entire frequency range.

In Figure 14 we compare the parameters obtained from the regression analysis and the prior mean values used in the analysis. As expected, the data significantly change the prior information for a_1 while the parameters a_2 and c_i are close to the prior mean value. Figure 15 shows plot of the source scaling term, $a_1 + a_2 M_w$, as a function of frequency and M_w . Note that the proposed model has the expected theoretical scaling since the scaling term is proportional to M_w for $f > 0.5$ Hz (*i.e.*, above the corner frequency of most events in the dataset) as expected from the ω^2 -source model. Note that the corner frequency in the source scaling term plots shift to lower frequencies as M_w increases as

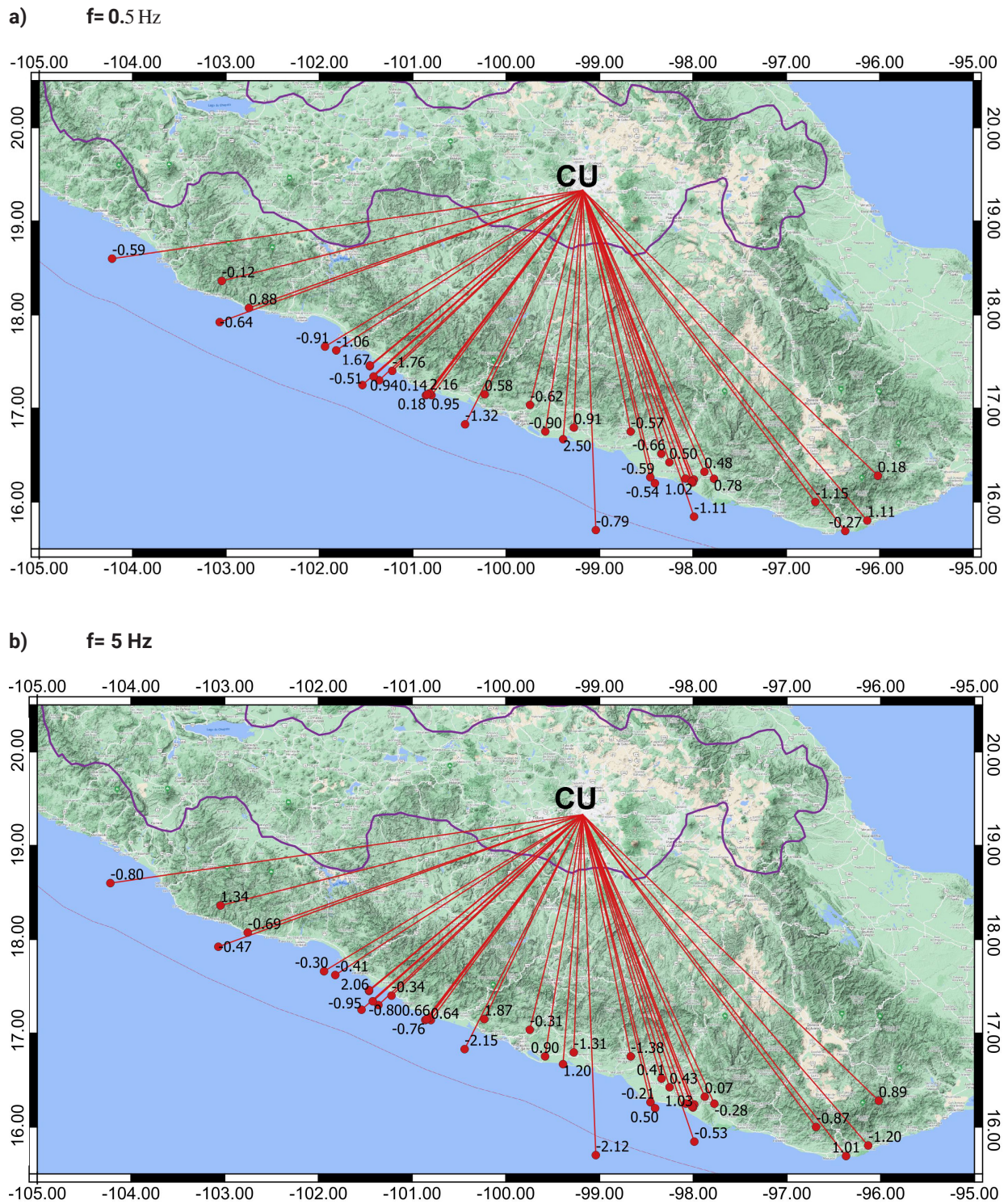


Figure 4. Map showing normalized residuals for the model defined in equation 2 at $f = 0.5 \text{ Hz}$ and $f = 5 \text{ Hz}$.

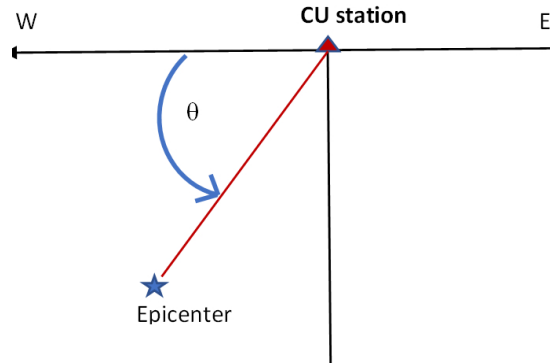


Figure 5. Definition of angle θ used in grouping events in bins.

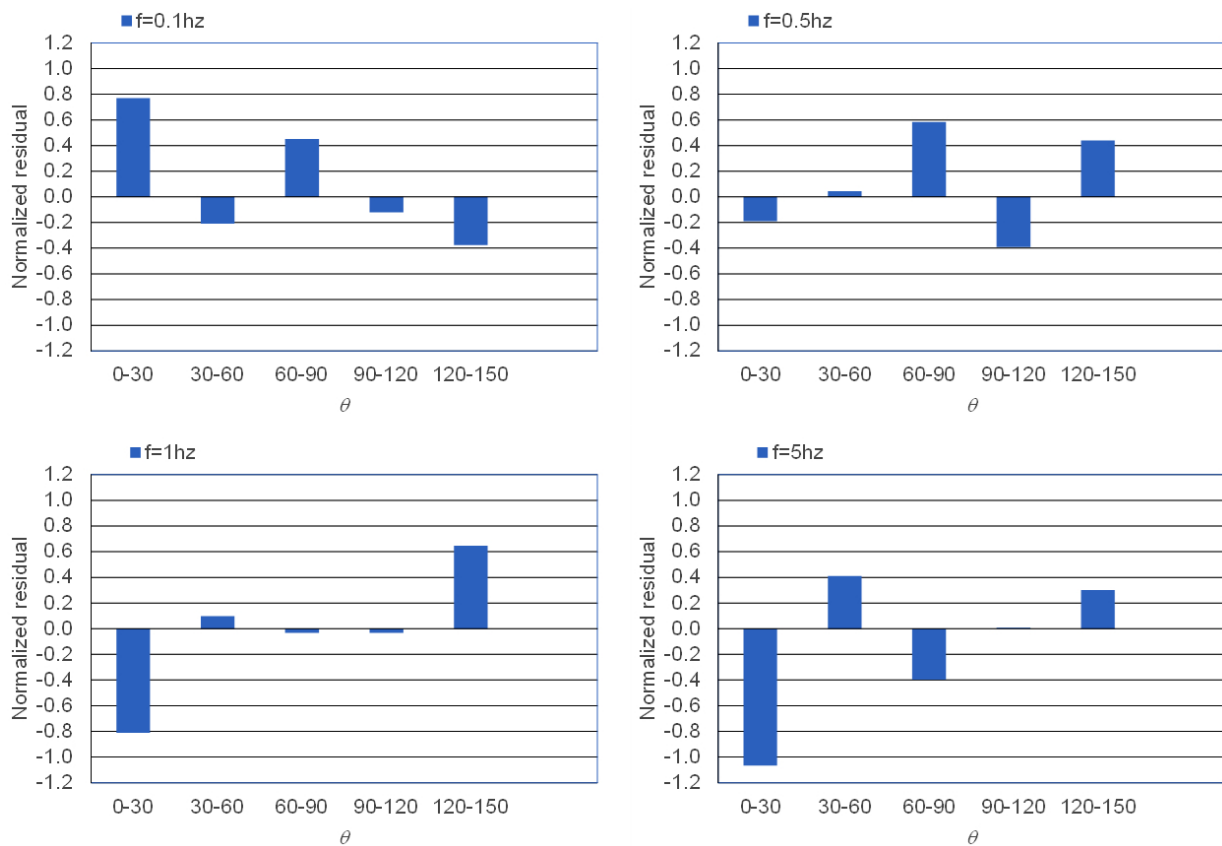


Figure 6. Variation of normalized residuals for the initial model defined in equation 2 with θ at selected frequencies.

Table 2. Coefficients for the proposed model in equation 4.

f, Hz	a ₁	a ₂	c ₁	c ₂	c ₃	c ₄	c ₅	σ
0.1	-7.4403	1.8508	-9.844E-04	-2.319E-03	-1.256E-03	-2.006E-03	-2.016E-03	0.717
0.11	-6.6177	1.7604	-8.730E-04	-2.394E-03	-1.357E-03	-2.066E-03	-2.256E-03	0.810
0.12	-6.7245	1.7985	-1.250E-03	-2.447E-03	-1.400E-03	-1.950E-03	-1.689E-03	0.762
0.13	-6.5159	1.7784	-1.525E-03	-2.497E-03	-1.403E-03	-1.533E-03	-1.790E-03	0.780
0.14	-6.3751	1.7715	-1.576E-03	-2.377E-03	-1.478E-03	-1.842E-03	-1.854E-03	0.755
0.15	-6.2226	1.7695	-1.261E-03	-2.518E-03	-1.742E-03	-1.685E-03	-1.650E-03	0.763
0.16	-6.2697	1.7921	-8.633E-04	-2.371E-03	-1.936E-03	-1.873E-03	-1.720E-03	0.797
0.17	-5.6027	1.7178	-7.225E-04	-2.968E-03	-2.158E-03	-1.430E-03	-9.503E-04	0.726
0.18	-5.2066	1.6711	-6.889E-04	-2.830E-03	-2.241E-03	-1.576E-03	-8.807E-04	0.797
0.19	-5.3646	1.7045	-9.875E-04	-2.771E-03	-2.223E-03	-1.579E-03	-1.098E-03	0.732
0.2	-4.7847	1.6192	-1.251E-03	-2.701E-03	-2.273E-03	-1.380E-03	-1.124E-03	0.744
0.21	-5.1450	1.6794	-1.501E-03	-2.144E-03	-2.239E-03	-1.326E-03	-1.537E-03	0.821
0.22	-5.5076	1.7561	-1.512E-03	-2.240E-03	-2.305E-03	-1.552E-03	-1.610E-03	0.702
0.24	-5.8537	1.8409	-1.586E-03	-2.336E-03	-2.246E-03	-2.219E-03	-1.530E-03	0.756
0.25	-6.0724	1.8843	-1.868E-03	-1.982E-03	-2.199E-03	-2.225E-03	-1.724E-03	0.753
0.26	-5.9307	1.8729	-2.346E-03	-1.751E-03	-2.208E-03	-2.191E-03	-1.245E-03	0.741
0.28	-5.2897	1.8310	-2.367E-03	-2.718E-03	-1.848E-03	-2.569E-03	-1.713E-03	0.643
0.29	-4.8379	1.7914	-2.285E-03	-2.878E-03	-1.899E-03	-2.647E-03	-2.110E-03	0.643
0.31	-5.0406	1.8565	-2.541E-03	-3.260E-03	-1.607E-03	-2.704E-03	-2.521E-03	0.600
0.33	-4.7300	1.8132	-2.796E-03	-3.411E-03	-1.704E-03	-2.185E-03	-2.809E-03	0.605
0.34	-4.5670	1.7881	-2.993E-03	-3.039E-03	-1.734E-03	-2.441E-03	-2.713E-03	0.662
0.36	-3.4665	1.6521	-2.719E-03	-3.426E-03	-1.716E-03	-3.336E-03	-2.920E-03	0.663
0.38	-3.1641	1.6241	-2.427E-03	-2.794E-03	-1.859E-03	-4.184E-03	-3.207E-03	0.694
0.4	-2.5956	1.5449	-2.286E-03	-3.277E-03	-1.534E-03	-4.323E-03	-3.352E-03	0.588
0.43	-2.4008	1.5016	-2.221E-03	-3.095E-03	-1.929E-03	-3.694E-03	-3.131E-03	0.566
0.45	-2.7788	1.5527	-2.240E-03	-3.113E-03	-2.411E-03	-3.593E-03	-2.443E-03	0.600
0.47	-2.4767	1.5077	-2.368E-03	-3.117E-03	-2.458E-03	-3.747E-03	-2.375E-03	0.601
0.5	-2.9118	1.6002	-3.300E-03	-2.884E-03	-1.994E-03	-3.667E-03	-2.621E-03	0.569
0.53	-2.0368	1.4916	-3.371E-03	-2.909E-03	-2.186E-03	-2.952E-03	-2.912E-03	0.621
0.56	-1.8736	1.4671	-3.029E-03	-3.383E-03	-2.377E-03	-2.368E-03	-3.194E-03	0.585
0.59	-1.5293	1.4160	-3.062E-03	-2.975E-03	-2.567E-03	-2.495E-03	-3.259E-03	0.527
0.62	-1.3190	1.3743	-3.369E-03	-2.870E-03	-2.337E-03	-2.588E-03	-3.378E-03	0.512
0.65	-1.2948	1.3627	-3.391E-03	-3.182E-03	-2.246E-03	-3.272E-03	-2.798E-03	0.556
0.69	-1.6501	1.3735	-3.787E-03	-2.866E-03	-2.243E-03	-2.972E-03	-2.688E-03	0.535
0.73	-1.0105	1.2993	-3.449E-03	-3.486E-03	-2.314E-03	-3.504E-03	-2.759E-03	0.438
0.77	-0.7145	1.2444	-3.961E-03	-3.163E-03	-2.615E-03	-3.573E-03	-3.169E-03	0.471
0.81	-0.6925	1.2456	-3.602E-03	-3.376E-03	-2.551E-03	-3.708E-03	-3.175E-03	0.483
0.85	-0.8940	1.2795	-3.288E-03	-3.776E-03	-2.800E-03	-3.513E-03	-3.437E-03	0.474
0.9	-0.7983	1.2449	-3.979E-03	-3.725E-03	-2.767E-03	-3.259E-03	-3.044E-03	0.476
0.95	-0.4314	1.1998	-3.708E-03	-3.570E-03	-2.986E-03	-3.256E-03	-2.391E-03	0.361
1	-0.3724	1.1938	-3.955E-03	-3.099E-03	-3.238E-03	-3.252E-03	-2.731E-03	0.379

1.06	-0.1406	1.1717	-3.648E-03	-3.673E-03	-3.548E-03	-3.222E-03	-2.896E-03	0.398
1.11	-0.5983	1.2292	-3.565E-03	-3.349E-03	-3.539E-03	-3.404E-03	-3.413E-03	0.396
1.18	-0.2920	1.1622	-3.999E-03	-3.526E-03	-3.595E-03	-3.271E-03	-3.673E-03	0.451
1.24	-0.3533	1.1848	-3.977E-03	-3.493E-03	-3.431E-03	-3.560E-03	-3.718E-03	0.393
1.31	-0.5841	1.1985	-4.070E-03	-3.581E-03	-3.533E-03	-3.783E-03	-3.818E-03	0.456
1.38	-0.6549	1.1979	-3.858E-03	-3.728E-03	-3.666E-03	-3.897E-03	-3.705E-03	0.434
1.46	-0.8558	1.2217	-4.194E-03	-3.718E-03	-3.529E-03	-3.915E-03	-4.109E-03	0.414
1.54	-0.6812	1.1945	-3.884E-03	-3.470E-03	-3.673E-03	-4.726E-03	-4.420E-03	0.456
1.62	0.4512	1.0231	-4.288E-03	-3.613E-03	-4.056E-03	-4.718E-03	-4.090E-03	0.495
1.71	-0.2807	1.1240	-4.115E-03	-3.489E-03	-4.163E-03	-4.821E-03	-4.049E-03	0.373
1.8	-0.4060	1.1424	-4.485E-03	-3.690E-03	-4.100E-03	-4.655E-03	-4.898E-03	0.439
1.9	-0.7700	1.1910	-4.929E-03	-3.749E-03	-4.168E-03	-4.314E-03	-4.778E-03	0.380
2.01	-0.2678	1.1171	-5.186E-03	-3.610E-03	-3.986E-03	-4.504E-03	-4.276E-03	0.438
2.12	-0.2912	1.0843	-5.061E-03	-3.231E-03	-4.426E-03	-4.227E-03	-4.528E-03	0.431
2.23	-0.6453	1.1221	-5.192E-03	-3.410E-03	-4.386E-03	-4.028E-03	-4.426E-03	0.371
2.36	-0.3661	1.0843	-5.480E-03	-4.149E-03	-4.235E-03	-4.962E-03	-4.993E-03	0.381
2.49	-0.6866	1.1225	-5.665E-03	-4.018E-03	-4.536E-03	-4.951E-03	-4.831E-03	0.421
2.62	-0.9134	1.1475	-5.405E-03	-3.765E-03	-4.652E-03	-5.326E-03	-4.713E-03	0.417
2.77	-0.6502	1.1277	-5.887E-03	-4.296E-03	-4.704E-03	-5.005E-03	-5.433E-03	0.392
2.92	-0.4173	1.0842	-5.601E-03	-4.124E-03	-5.225E-03	-4.838E-03	-5.671E-03	0.401
3.08	-0.3605	1.0667	-5.800E-03	-4.240E-03	-4.829E-03	-5.237E-03	-5.258E-03	0.358
3.25	0.1369	0.9903	-6.171E-03	-4.410E-03	-5.109E-03	-4.768E-03	-5.365E-03	0.405
3.43	-0.1349	1.0454	-6.304E-03	-4.588E-03	-5.269E-03	-5.265E-03	-6.139E-03	0.382
3.62	-0.2889	1.0658	-6.490E-03	-4.720E-03	-5.257E-03	-5.746E-03	-5.929E-03	0.388
3.82	-0.3401	1.0517	-6.582E-03	-4.094E-03	-5.673E-03	-5.468E-03	-5.547E-03	0.398
4.03	0.0017	1.0012	-6.596E-03	-4.563E-03	-5.656E-03	-5.255E-03	-5.680E-03	0.415
4.25	-0.3213	1.0429	-6.893E-03	-4.280E-03	-5.660E-03	-5.675E-03	-6.245E-03	0.367
4.48	-0.2932	1.0474	-7.330E-03	-4.691E-03	-5.839E-03	-5.906E-03	-6.115E-03	0.411
4.73	-0.3853	1.0211	-7.217E-03	-4.323E-03	-5.916E-03	-5.589E-03	-5.765E-03	0.421
4.99	-0.5101	1.0355	-7.464E-03	-4.736E-03	-5.567E-03	-5.778E-03	-6.352E-03	0.406
5.26	-0.1366	0.9754	-7.762E-03	-5.065E-03	-6.244E-03	-5.803E-03	-6.244E-03	0.439
5.55	-0.2660	0.9927	-7.611E-03	-5.219E-03	-6.527E-03	-6.515E-03	-6.453E-03	0.482
5.86	-0.5841	1.0228	-8.059E-03	-5.499E-03	-6.308E-03	-6.966E-03	-6.549E-03	0.434
6.18	-0.5244	1.0129	-8.025E-03	-5.508E-03	-6.664E-03	-7.343E-03	-6.865E-03	0.450
6.52	-0.3751	0.9996	-8.122E-03	-5.897E-03	-7.004E-03	-7.470E-03	-7.275E-03	0.466
6.88	-0.5177	0.9992	-8.224E-03	-5.907E-03	-6.991E-03	-7.160E-03	-6.878E-03	0.485
7.25	-0.5989	1.0180	-8.417E-03	-6.332E-03	-7.224E-03	-7.461E-03	-7.169E-03	0.495
7.65	-0.6367	1.0047	-8.463E-03	-6.498E-03	-7.386E-03	-7.704E-03	-7.225E-03	0.504
8.07	-0.9273	1.0164	-8.332E-03	-6.726E-03	-7.417E-03	-7.686E-03	-7.268E-03	0.513
8.52	-1.4988	1.0681	-8.046E-03	-6.836E-03	-7.468E-03	-7.487E-03	-7.398E-03	0.533
8.98	-1.2225	1.0085	-7.988E-03	-7.000E-03	-7.878E-03	-8.107E-03	-7.757E-03	0.560
9.48	-1.3279	1.0133	-8.033E-03	-7.878E-03	-8.087E-03	-8.469E-03	-7.988E-03	0.609
10	-1.3478	0.9877	-7.601E-03	-8.019E-03	-8.359E-03	-8.733E-03	-8.032E-03	0.667

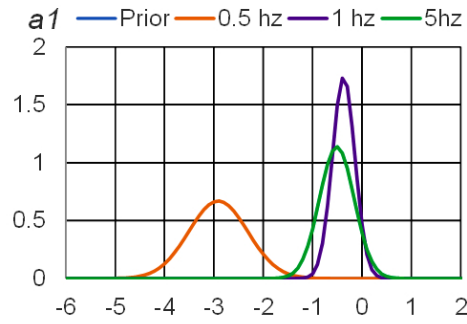


Figure 7. Comparison of posterior probability density functions for parameter a_1 for $f=0.5, 1$ and 5 Hz. The prior probability density function was a normal density with a very large variance for all frequencies, therefore it is not visible in the figure because of the scale.

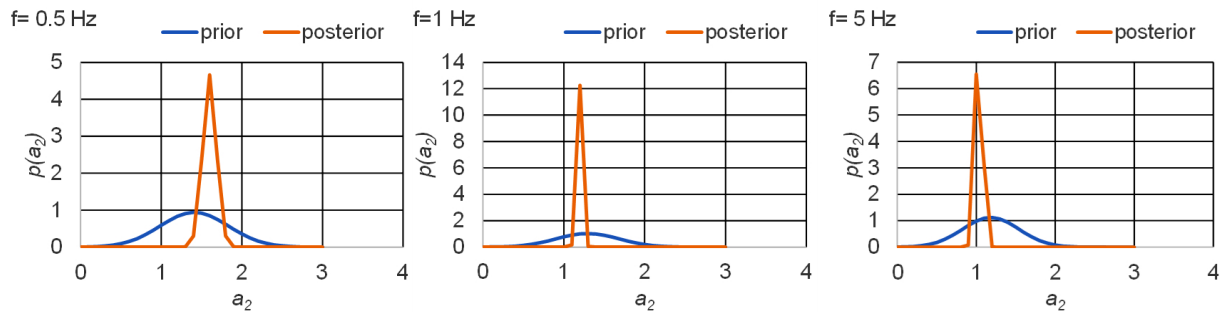


Figure 8. Prior and posterior probability density functions for a_2 parameter for $f=0.5, 1$ and 5 Hz.

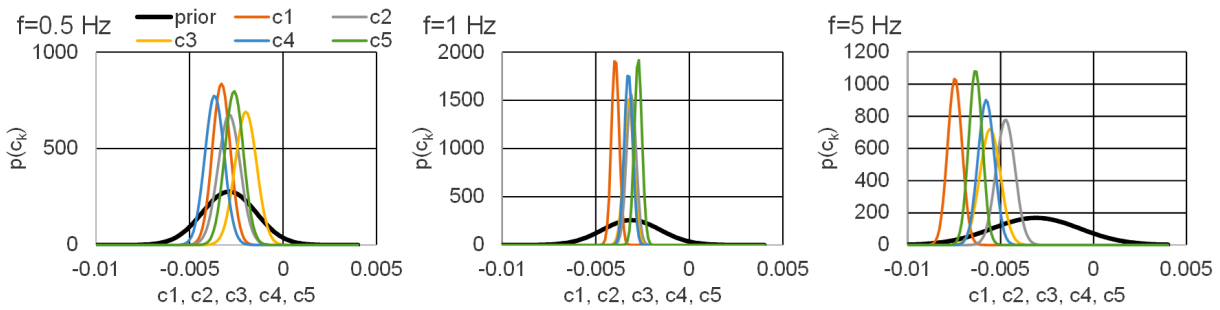


Figure 9. Prior and posterior probability density functions for c_1, c_2, c_3, c_4 and c_5 parameters for $f=0.5, 1$ and 5 Hz.

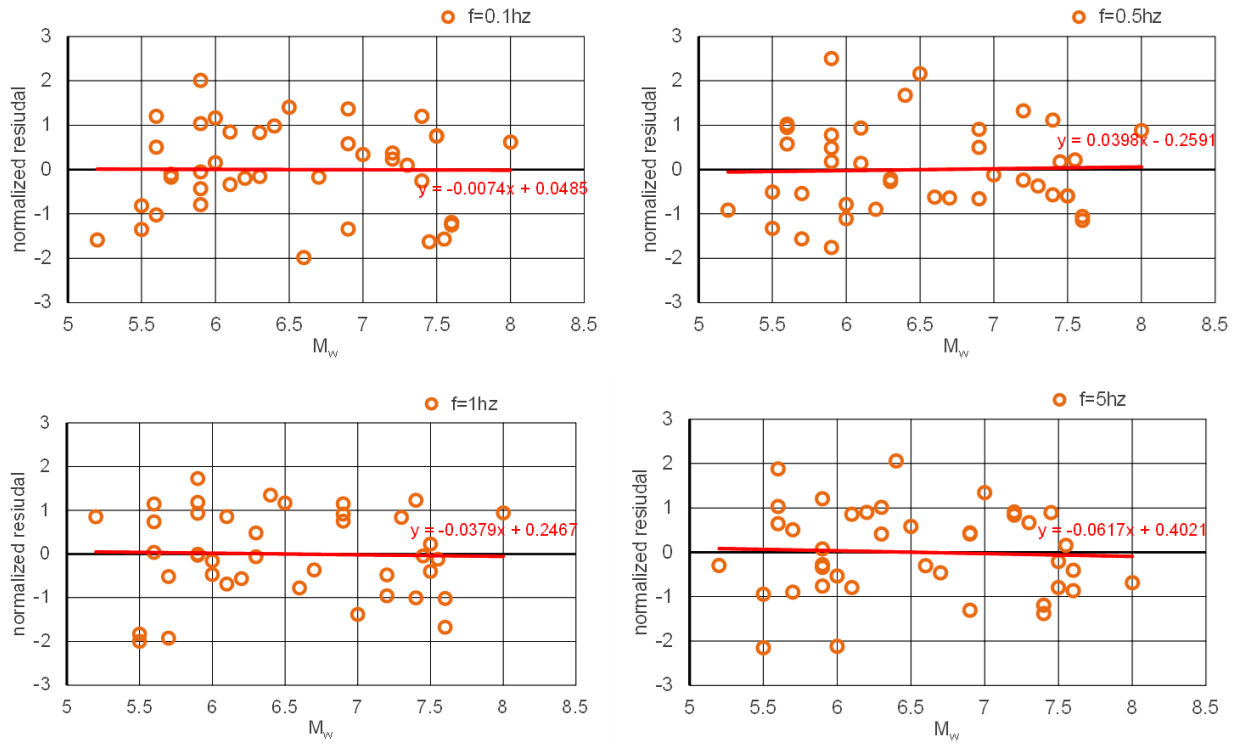


Figure 10. Normalized residuals as a function of M_w for the proposed model (equation 4).

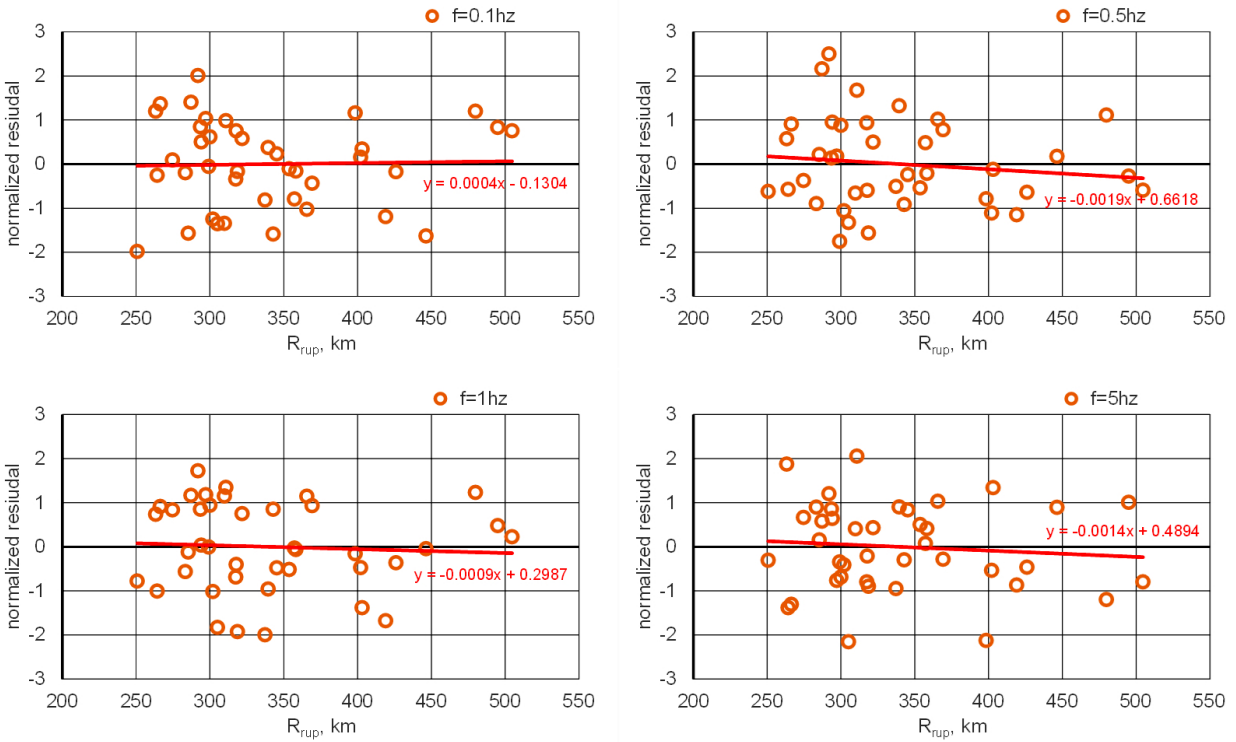
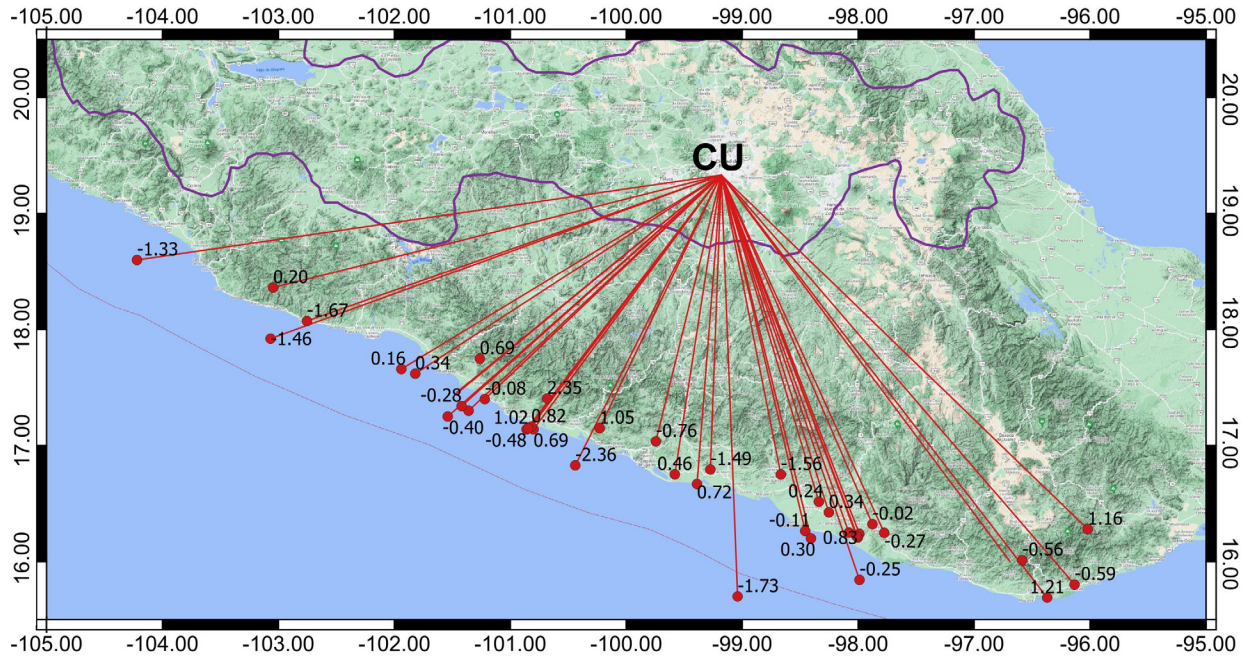


Figure 11. Normalized residuals as a function of R_{rup} for the proposed model (equation 4).

a) $f = 0.5 \text{ Hz}$



b) $f = 5 \text{ Hz}$

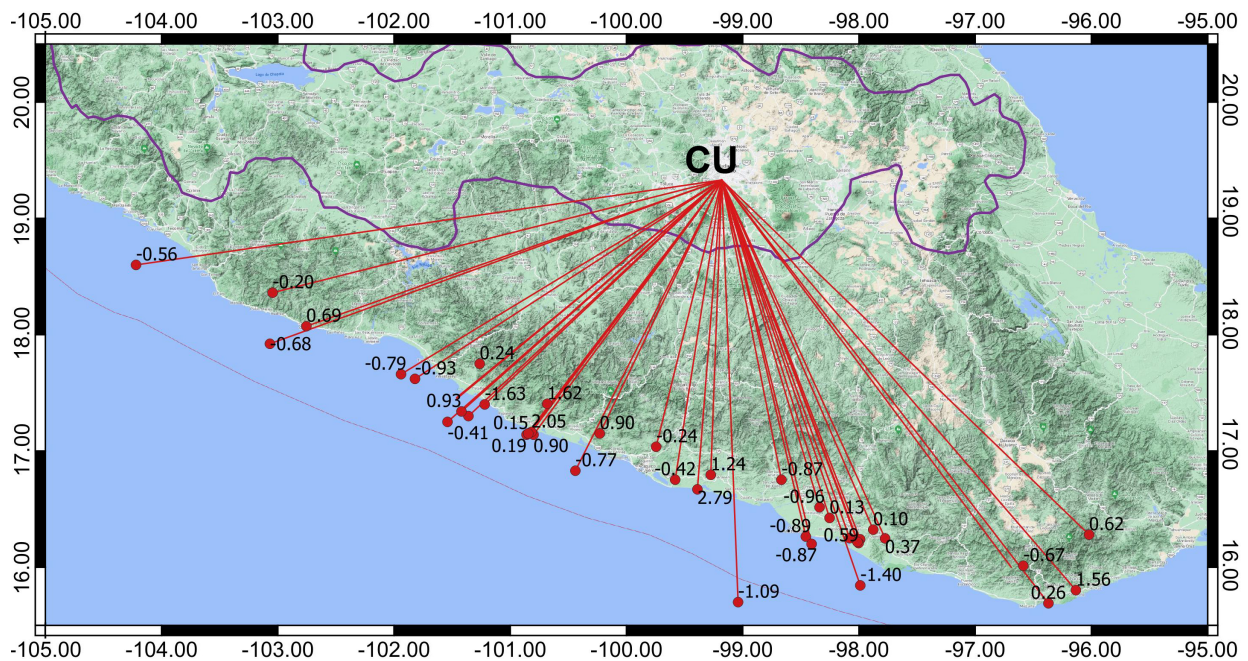


Figure 12. Map showing normalized residuals for the proposed model (equation 4) at $f = 0.5 \text{ Hz}$ and $f = 5 \text{ Hz}$.

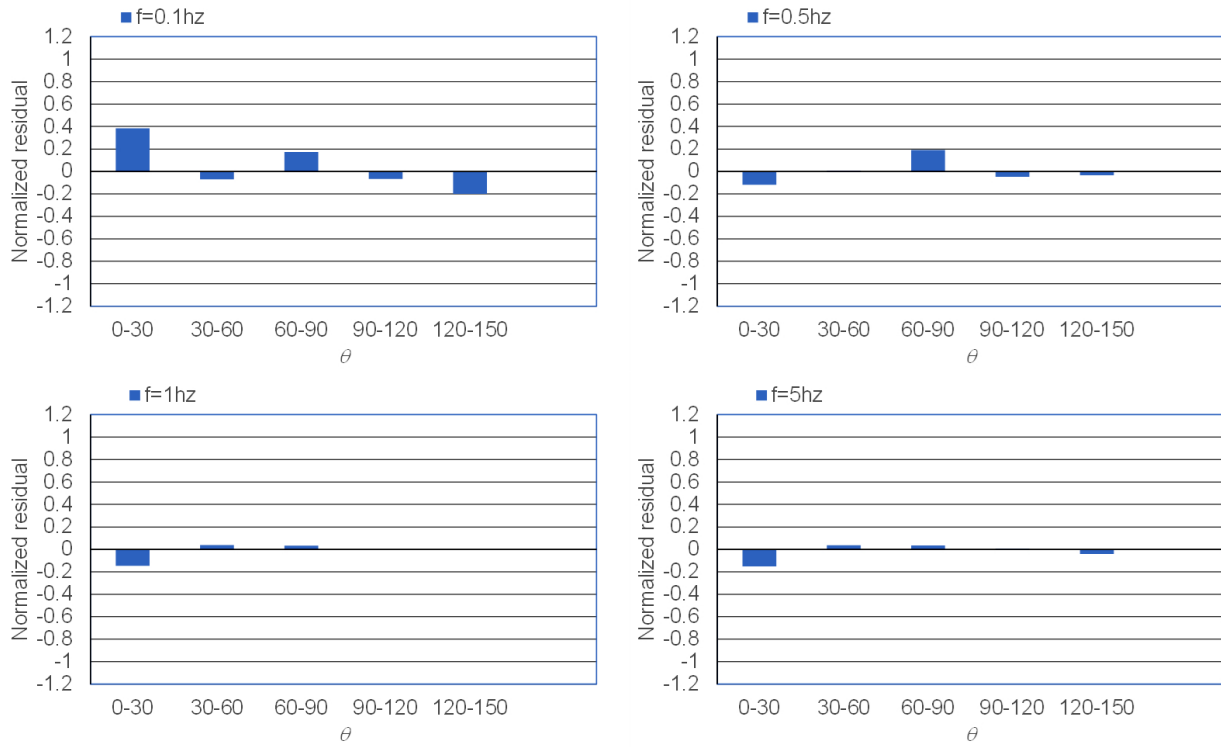


Figure 13. Variation of normalized residuals for the proposed model (equation 4) with θ at selected frequencies.

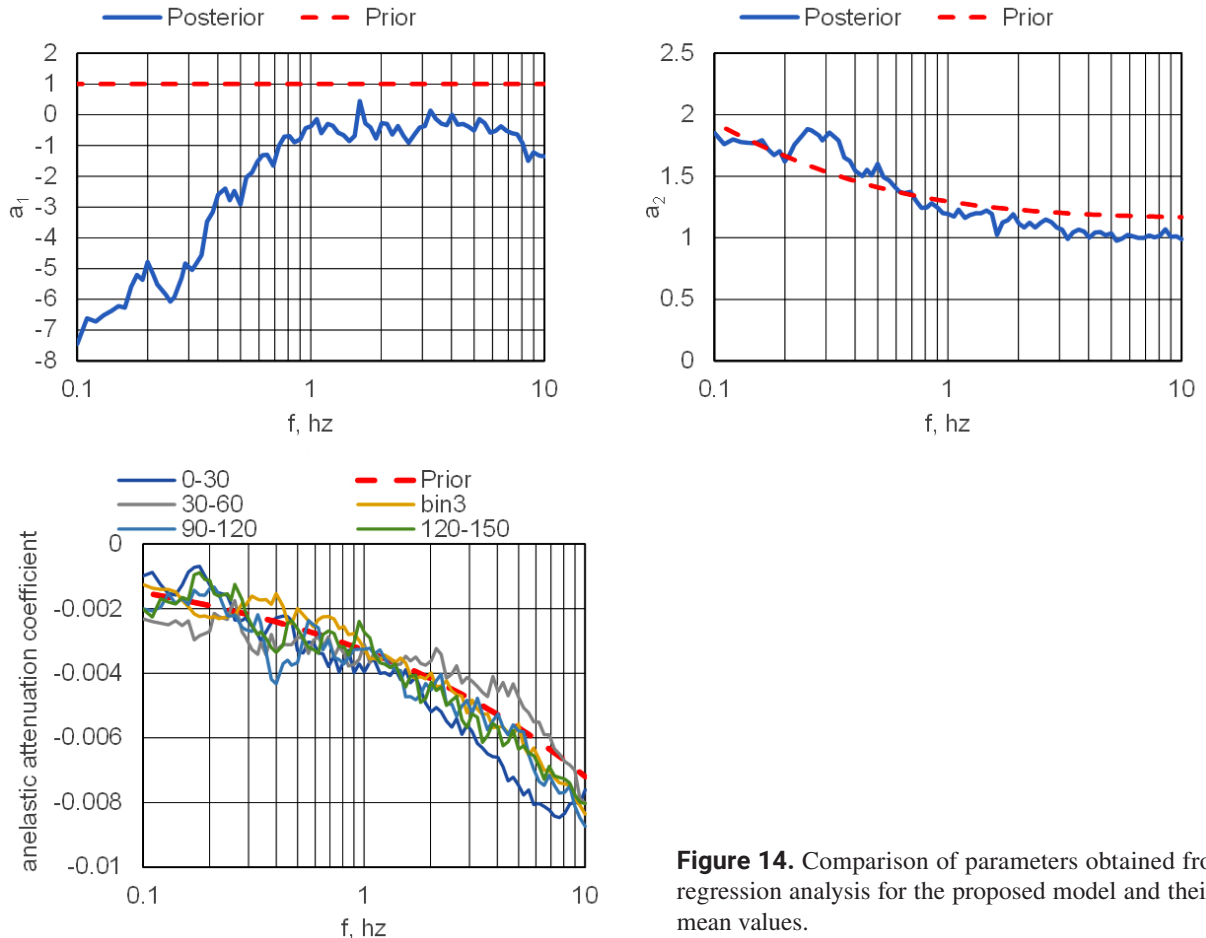


Figure 14. Comparison of parameters obtained from the regression analysis for the proposed model and their prior mean values.

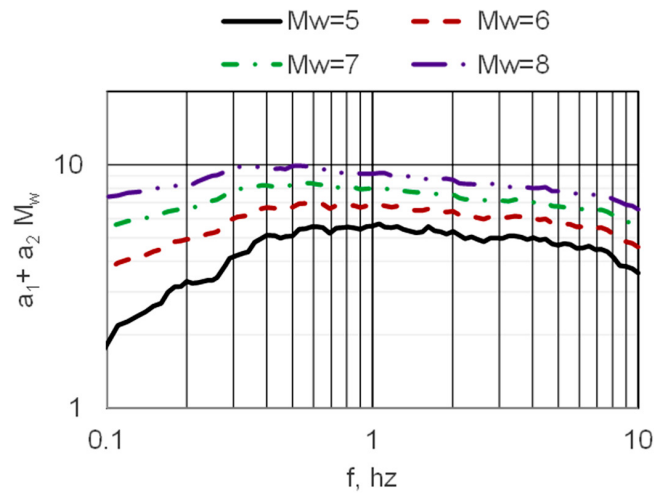


Figure 15. Source scaling term ($a_1 + a_2 M_w$) as function of frequency and M_w for the proposed model (equation 4). Note that the scaling term is roughly proportional to M_w for $f > 0.5$ Hz (i.e., above the corner frequency of most events in the dataset) as expected from the ω^2 -source model.

expected from the seismological theory. In Figure 16 we show the magnitude scaling of *FAS* predictions for a distance of 300 km, note that magnitude scaling is the same for all distances according to the proposed model. However, in view that earthquakes being analyzed herein always happen at distances larger than 200 km the magnitude scaling in Figure 16 seems reasonable.

In Figure 17 we compare σ values reported by Ordaz *et al.* (1994) (based on the model given in equation 2), and those obtained in this study (based on the proposed model given in equation 4). Clearly a significant reduction in σ values is obtained with the proposed model. This is a valuable characteristic of the proposed model because it leads to a better estimation of seismic hazard. The reduction in σ values partly comes from the increase in the quality and quantity of records and partly from the functional form that we used to model different anelastic attenuation along different ray paths.

Figure 17 also shows σ values for the model in equation 2 but including the new data. The significant reduction in σ for the model in equation 2 with respect to the model of Ordaz *et al.* (1994) is produced due to the increase in the quality and quantity of the dataset, while the reduction in σ for the proposed model with respect to the model in equation 2 is the result of the modeling of different attenuation along different ray paths. Note that the reduction in σ for the proposed model with respect to the model in equation 2 is present for all frequencies but is slightly more pronounced at higher frequencies. Finally, we note that a simple modification to the functional form leads to a reduction in the aleatory variability of the GMPE. As discussed before on

important application of the model is to estimate the value of seismic intensities during future earthquakes (i.e. PGA, PGV and SA). Therefore, we performed several test and we identified that for the ground motions in Mexico City the range of frequencies considered in the model is sufficient to estimate the seismic intensities in the framework of random vibration theory.

4. Comparison of Observations and Predictions from the Proposed GMPE

In Figure 18 we show a comparison of the observed and predicted *FAS* for some of the earthquakes in the dataset. In general, the GMPE curves fit the observed *FAS* well. Two of the exceptions are the observed *FAS* for the Guerrero earthquakes of 08/05/2014 (M_w 6.5) and 10/05/2014 (M_w 6.1) which are greater than the predicted *FAS*. This agrees with the strong directivity towards Mexico City during these two earthquakes documented by Singh *et al.* (2019). Figure 18 also includes the Acapulco earthquake of 08/09/2021 (M_w 7.0), and Michoacán - Colima earthquakes of 19/09/2022 (M_w 7.6) and 22/09/2022 (M_w 6.7) which were not included in the regression analysis. The model fits well the 19/09/2022 (M_w 7.6) earthquake but underestimates the earthquakes of 08/09/2021 (M_w 7.0) and 22/09/2022 (M_w 6.7) both of which are known to have ruptured towards Mexico City (Iglesias *et al.* 2022; Singh *et al.*, 2023).

Figure 19 shows a comparison of *FAS* at CU for a postulated M_w 8.0 earthquake at $R_{rup}=300$ km located in different θ bins.

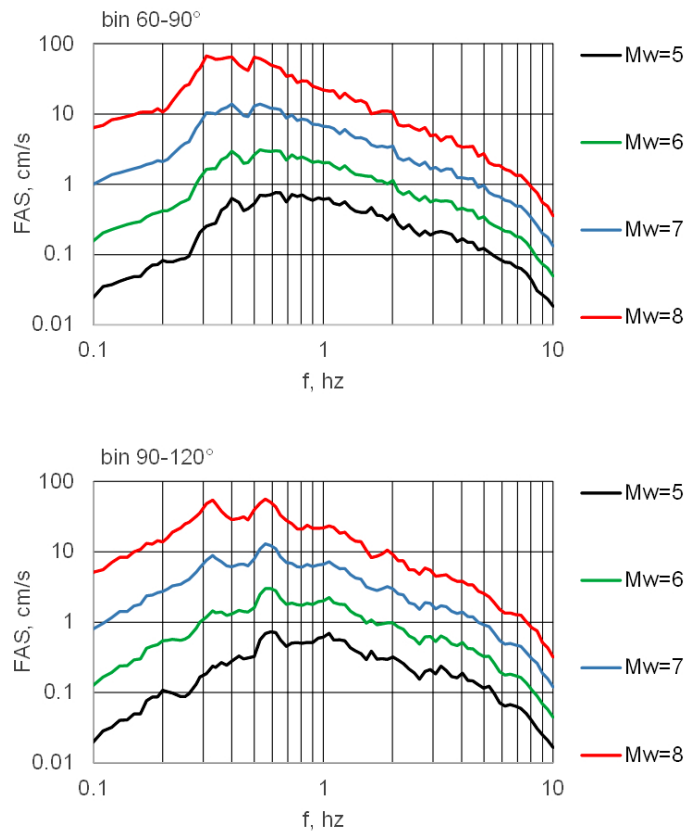


Figure 16. Scaling for *FAS* predictions with M_w for a distance of 300 km.

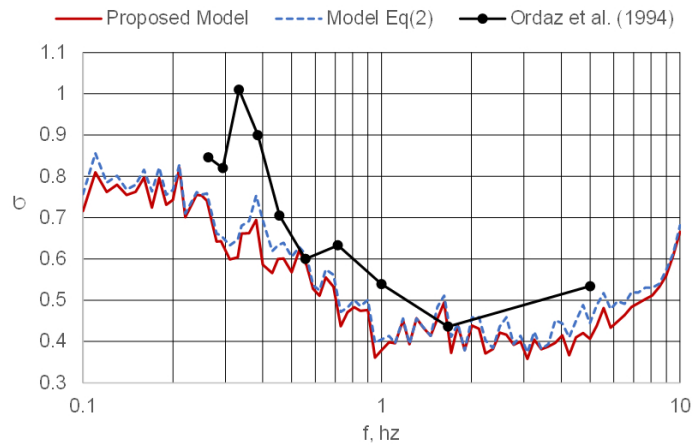


Figure 17. Comparison of σ for different models. σ for the proposed model (equation 4) is less than for the initial model (equation 2) which, in turn, is smaller than for the model of Ordaz *et al.* (1994).

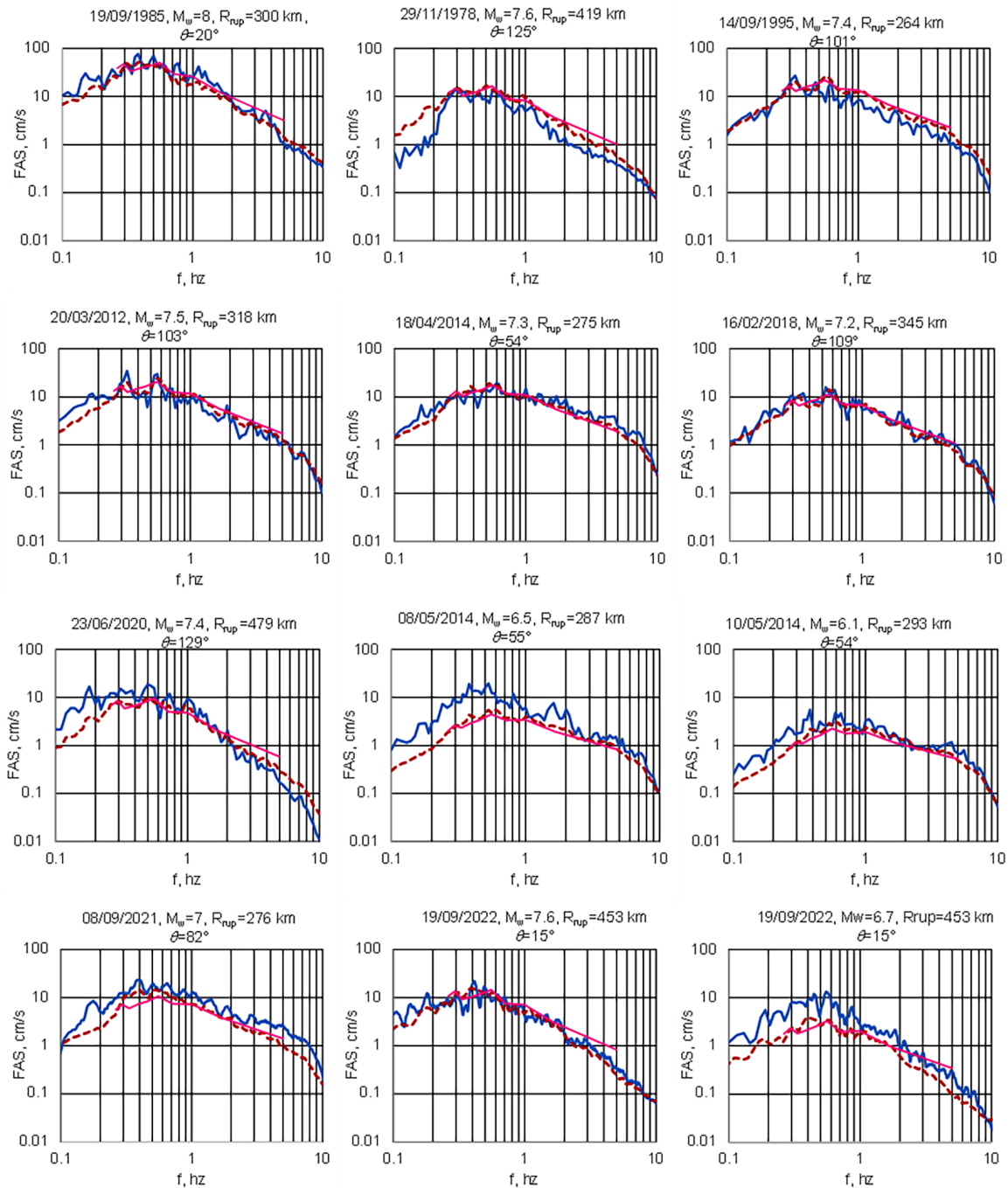


Figure 18. Comparison of observed (continuous curves), predicted (dashed red curves) *FAS* from the proposed model and predicted (pink continuous line) *FAS* from the Ordaz *et al.* (1994) GMPE for some of the earthquakes in the dataset. Predicted *FAS* are from the new model (equation 4). Note that the recent Acapulco earthquake of 08/09/2021 (M_w 7.0) and Michoacán - Colima earthquakes of 19/09/2022 (M_w 7.6) and 22/09/2022 (M_w 6.7) were not used in the regression analysis for the proposed model. While only the recordings during the 19/09/1985 (M_w 8) and the 29/11/1978 (M_w 7.6) earthquakes were used in the regression analysis for the Ordaz *et al.* (1994) model.

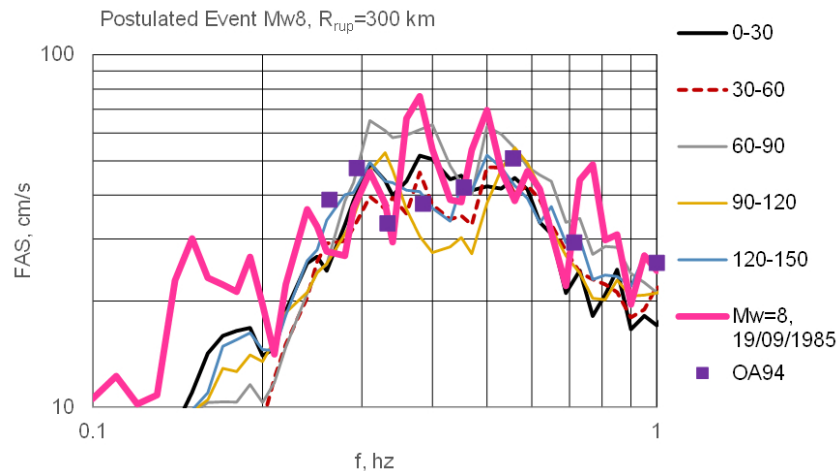


Figure 19. Predicted *FAS* at CU from an M_w 8.0 earthquake at $R_{rup} = 300$ km located in different θ bins. For comparison, the observed *FAS* of the 1985 Michoacán earthquake, M_w 8.0, $R_{rup} = 300$ km ($\theta = 20^\circ$) is shown. The purple squares are predictions from the Ordaz *et al.* (1994) GMPE.

The model predicts larger intensities from earthquakes from the 60° - 90° bin, a region that includes San Marcos and Papanoa seismic sources, and from the 0° - 30° bin, a region that includes Michoacán seismic source. Unfortunately, our study suggest that such regions have the potential to produce SM at Mexico City comparable to ground motions observed during the deadly 1985 M_w 8.0 Michoacán earthquake.

5. Conclusions

The estimation of strong ground motion at CU from future earthquakes is crucial for seismic hazard assessment of Mexico City. In this study, we have taken advantage of the recent increase in the number of earthquakes that have produced recordings at CU to derive a site-specific GMPE for *FAS* from subduction thrust faulting interface earthquakes. The dataset is composed of 40 earthquakes ($5 \leq M_w \leq 8$) at distances between 250 and 500 km. We used a functional form based on a point-source model but included a modification to model different attenuation along different ray paths. We show that this simple modification leads to a significant reduction in the aleatory variability of the GMPE particularly at frequencies greater than 1 Hz. The model is applicable to *FAS* in CU station in Mexico City during thrust faulting interface earthquakes with M_w between 5 and 8 and distances in the range between 250 and 500 km. The proposed model has been incorporated in a fully Fourier-based PSHA for Mexico City leading to earthquake design spectra in the 2023 version of the Mexico City Building Code.

6. Acknowledgments

A functional form similar to equation 4 was proposed many years ago by Eduardo Pérez-Rocha and others. This study was supported by Instituto para la Seguridad de las Construcciones de la CDMX and by DGAPA, UNAM project IN109423 (S.K.S.). Authors thank also the two reviewers who provided constructive criticism for the initial version of this manuscript that allowed its improvement.

7. References

- Anderson, J. G., P. Bodin, J. Brune, J. Prince, S. K. Singh, R. Quass, and M. Oñate. (1986). Strong ground motion from the Michoacan, Mexico earthquake, *Science* 233, 1043-1049. doi: <https://doi.org/10.1126/science.233.4768.1043>
- Arroyo, D., García, D., Ordaz, M., Mora, M. A., & Singh, S. K. (2010). Strong ground-motion relations for Mexican interplate earthquakes. *Journal of Seismology*, 14, 769-785. Doi: <https://doi.org/10.1007/s10950-010-9200-0>
- Boore, D.M. (2003). Simulation of ground motion using the stochastic method, *Pageoph* 160, 635-676. doi: <https://doi.org/10.1007/PL00012553>
- Broemling, L.D., (1985). *Bayesian Analysis of Linear Models*, Marcel Dekker, Inc., New York. doi: <https://doi.org/10.1201/9781315138145>
- Brune, J.N (1970). Tectonic stress and the spectra of seismic shear waves from earthquakes, *J. Geophys. Res.* 75, 4997-5009. doi: <https://doi.org/10.1029/jb075i026p04997>
- Castro, R., S. K. Singh, and E. Mena (1988). An empirical model to

- predict Fourier amplitude spectra of horizontal ground motion, *Earthquake Spectra* 4, 675-686. doi: <https://doi.org/10.1193/1.1585497>
- Celebi, M., J. Prince, C. Dietel, M. Oñate, and G. Chavez (1987). The culprit in Mexico City-amplification of motions, *Earthquake Spectra* 3, 315-328. doi: <https://doi.org/10.1193/1.1585431>
- Cruz-Atienza, V. M. et al. (2016). Long duration of ground motion in the paradigmatic Valley of Mexico, *Sci. Rep.* 6, 38807. doi: <https://doi.org/10.1038/srep38807>
- García, D., Singh, S. K., Herráiz, M., Ordaz, M., & Pacheco, J. F. (2005). Inslab earthquakes of central Mexico: peak ground-motion parameters and response spectra. *Bulletin of the Seismological Society of America*, 95(6), 2272-2282. doi: <https://doi.org/10.1785/0120050072>
- Iglesias, A., S.K. Singh, J.F. Pacheco, L. Alcántara, M. Ortiz, and M. Ordaz (2003), Near-trench Mexican earthquakes have anomalously low peak accelerations, *Bull. Seism.Soc. Am.*, 93, 953-959. doi: <https://doi.org/10.1785/0120020168>
- Joyner, W. J. and D. M. Boore (1986). On simulation of large earthquakes by Green's functions addition of small earthquakes. In Das S, Boatwright J, Scholtz C H (ed) *Earthquake Source Mechanics*, (Maurice Ewing Series 6). *American Geophysical Union Monograph* 37, Washington, D.C., 269-274. doi: <https://doi.org/10.1029/GM037p0269>
- Kanamori H, P. C. Jennings, S. K. Singh, and L. Astiz (1993). Estimation of strong ground motions in Mexico City expected for large earthquakes in the Guerrero seismic gap. *Bull Seism Soc. Am.* 93, 811-829. doi: <https://doi.org/10.1785/BSSA0830030811>
- Ordaz, M. and Singh, S.K., (1992). Source spectra and spectral attenuation of seismic waves from Mexican earthquakes, and evidence of amplification in the hill zone of Mexico City, *Bull Seism Soc. Am.* 82, 24-43. doi: <https://doi.org/10.1785/BSSA0820010024>
- Ordaz, M., S. K. Singh, and A. Arciniega (1994). Bayesian attenuation regressions: an application to Mexico City, *Geophys. J. Int.*, 177, 335- 344. doi: <https://doi.org/10.1111/j.1365-246X.1994.tb03936.x>
- Ordaz, M., J. Arboleda, and S. K. Singh (1995). A scheme of random summation of an empirical Green's function to estimate ground motions from future large earthquakes. *Bull Seism Soc. Am.* 85, 1635-1647. doi: <https://doi.org/10.1785/BSSA0850061635>
- Ordaz, M., E. Reinoso, M. A. Jaimes, L. Alcántara, and C. Pérez (2017). High-resolution early earthquake damage assessment system for Mexico City based on a single-station, *Geofísica Internacional.* 56, 117-135. doi: <https://doi.org/10.22201/igeof.00167169p.2017.56.1.1751>
- Rosenblueth, E. (1953). *Teoría del diseño sísmico sobre mantos blandos*, Ediciones ICA, Serie B, No. 14, 3-12.
- Shapiro, N.M., S.K. Singh, and J.F. Pacheco (1998). A fast and simple diagnostic method for identifying tsunamigenic earthquakes, *Geophys. Res. Lett.* 25, 3911-3914. doi: <https://doi.org/10.1029/1998GL900015>
- Singh, S. K., J. Lermo, T. Domínguez, M. Ordaz, J. M. Espinosa, E. Mena, and R. Quaa (1988a). A study of relative amplification of seismic waves in the Valley of Mexico with respect to a hill zone site (CU), *Earthquake Spectra* 4, 653-674. doi: <https://doi.org/10.1193/1.1585496>
- Singh, S. K., E. Mena, and R. Castro (1988b). Some aspects of source characteristics of 19 September 1985 Michoacan earthquake and ground motion amplification in and near Mexico City from the strong motion data, *Bull. Seism. Soc. Am.* 78, 451-477. doi: <https://doi.org/10.1785/BSSA0780020451>
- Singh, S.K., Arroyo, D., Pérez-Campos, X., Rodríguez, Q, and Iglesias, A. (2016). Fast identification of near-trench earthquakes along the Mexican subduction zone based on characteristics of ground motion in Mexico City, *Bull. Seism. Soc. Am.* 106, 2071-2080, doi: <https://doi.org/10.1785/0120160003>
- Singh, S.K., E. Reinoso, D. Arroyo, M. Ordaz, V. Cruz-Atienza, X. Pérez-Campos, A. Iglesias, and V. Hjörleifsdóttir (2018). Deadly intraslab Mexico earthquake of 19 September 2017 (Mw7.1): Ground motion and damage pattern in Mexico City, *Seism. Res. Lett.* 89, 2193-2203, doi: <https://doi.org/10.1785/0220180159>
- Singh, S.K., Plata-Martínez, R., Pérez-Campos, X., Espíndola, V., Arroyo, D. and Iglesias, A. (2019). Evidence of directivity during the earthquakes of 8 and 10 May 2014 (Mw 6.5, 6.1) in the Guerrero, Mexico seismic gap and some implications, *J. Seism.* 23, 683-697.
- Singh, S. K., Iglesias Mendoza, A., Arroyo, D., Pérez-Campos, X., Ordaz, M., Mendoza, C., Corona-Fernández, R. D., Espíndola, V. H., González-Ávila, D., Martínez-López, R., Castro-Artola, O., Santoyo, M. A., & Franco, S. I. (2023). A Seismological study of the Michoacán-Colima, Mexico, Earthquake of 19 September 2022 (Mw7.6). *Geofísica Internacional*, 62(2), 445-465. doi: <https://doi.org/10.22201/igeof.2954436xe.2023.62.2.1453>